JMEPEG (2005) 14:395-407
DOI: 10.1361/10599490523869

1059-9495/$19.00

Interaction Analysis of the Twin-Roller Strip-Casting Process and the Implications for Process Control

John B. Edwards and Alberto Cavazos

(Submitted October 26, 2004; in revised form December 22, 2004)

Twin-roller steel strip casting may offer advantages with respect to classic continuous-casting hot-rolling processes. Only a few studies have reported control aspects of this process, and, although successful, little attention has been given to the interactions between variables. In this study, the derivation of a 3 × 3 linearized multivariable model for process control purposes that has been proposed in previous investigations is presented. The model was simplified to a 2 × 2 plant. The process was found to be highly interactive and nonlinear, involving time delays. An analysis of interactions and their implications for process control is also presented. The multivariable model proposed was successfully used for multivariable control design in subsequent works.

Keywords: multivariable systems, process modeling, steel industry, strip casting

1. Introduction

Continuous strip casting offers industry the opportunity to reduce production costs, energy consumption, and the loss of material by partial or total elimination of subsequent shaping stages. The capital cost will also be reduced as a result of the installation of low-head machines and the elimination of roughing stands in strip mills (Ref 1, 2). The need for highly responsive interactive control is a consequence of the reduction in storage capacity of the strip caster in comparison with traditional processes. These processes can also bring an improvement in uniformity quality and new properties to the final steel.

The twin-roller strip-casting process is suitable to directly cast a thin strip with a thickness between 1 and 5 mm, and even thinner (Ref 3). However, successful implementation is very much dependent on the highly interactive processes of heat and fluid flow, and, therefore, on the control of heat and flow extraction. The solidification rate has to be controlled to allow good mechanical properties of the final product, and to avoid surface cracking and faults in the structure of the solidified steel as well as the so-called *breakout problem.*

Various works on the modeling and control of twin-roller casters have been reported in the literature. Although successful, little attention has been given to the multivariable aspect of the process (i.e., the interaction between loops) (Ref 4-13). Some authors claim to have implemented successful controls; however, no details were given (Ref 4, 5). Several single-loop controllers have been proposed: the strip thickness was controlled via a force control (Ref 6) and by using a gain schedule proportional plus integral (PI) controller (Ref 6, 7), while fuzzy controllers have been proposed for molten steel levels (Ref 8, 9). More recent works have proposed a two-level control (Ref 10, 11). Three local controllers are designed for the molten steel level, roll gap, and roll speed. Interactions are treated as disturbances from the other systems; however, because this is not enough to achieve a constant roll separation force, a high-level (supervisory) controller is then required.

In previous investigations within the Department of Automatic Control and Systems Engineering (ACSE) of the University of Sheffield, some nonlinear static relations have been derived and validated in a real-life caster (Ref 14). The process was found to be highly interactive and nonlinear with the presence of unbreakable delay-integrator loops. Consequently, a 3 × 3 linearized model suitable for control analysis and design was derived. Nonetheless, in the early works only diagonal controllers were proposed. The model was simplified to a 2 × 2 size on a justified basis, and a time-domain (step response) multivariable analysis was performed (Ref 15). One of the conclusions was the multivariable approach becomes crucial due to the high level of interactions. A full multivariable analysis and the application of several multivariable control techniques, with the aim of reducing interactions, were performed (Ref 16). The multivariable control techniques used were the Owens first-order approximations (Ref 17), an H_∞-optimal control for nominal performance (Ref 18), and the multivariable Smith predictor of Alevisakis and Seborg (Ref 19). The effects of the nonlinearities were addressed by changing the operating conditions. A real-time simulator based on the model was also built (Ref 20).

Shell growth is described by Eq 1, which is one of the main contributions of earlier investigations on the twin-roller caster at the University of Sheffield (Ref 14, 20). The shell growth was modeled using similar principles and leads to similar results, although different representations have been used (Ref 6, 7, 10-12). However, the present work is concerned with the model of the cross-coupling elements, such as molten steel level (or molten steel input flow) to roll separation force, and, hence, the interaction effects that have not been specifically addressed. The derivation of the multivariable 3 × 3 model for

John B. Edwards, University of Sheffield, Mappin Street, Sheffield S1 4UD, United Kingdom; and **Alberto Cavazos,** Universidad Autónoma de Nuevo León cd. Universitarra San Nicolés de les G. 66451 México. Contact e-mail: acavazos@fime.uanl.mx.

the control of the twin-roller strip-casting process, as well as the simplification to a 2 × 2 model, is presented. The interactions are analyzed via some of their multivariable characteristics, such as multivariable poles and zeros, interaction ratios, singular values, and minimized condition numbers. The implications for process control are discussed.

The validation of the model in a real-life caster is not presented here (Ref 14). However, the model was calibrated according to a pure static model that has been in use at an industrial site and was experimentally validated. This model has been used satisfactorily, and it is considered to be a good approximation of the plant during steady state. The real-time simulator was validated with real-life data (Ref 20).

2. Twin-Roller Strip-Casting Process

Twin-roller strip casting consists of feeding molten metal directly into a gap between two horizontal cooling rollers that are rotating in opposite directions in such a way that the melt is led through the gap (Fig. 1). The gap between rollers (x_g) approximates the thickness of the desired product. A pool of molten steel is formed within the gap between the rollers as the melt is fed into the system. The steel then solidifies progressively along the arc of contact with the cooling roller surface. The molten and solid steel, in an idealized manner, are separated by a line forming a shell, as shown in Fig. 1. The point at

Nomenclature

$\overline{\sigma}(j\omega)$	maximum singular value
$\overline{\sigma}(M)$	maximum singular value of a matrix M
$\underline{\sigma}(j\omega)$	minimum singular value
$\underline{\sigma}(M)$	minimum singular value of a matrix M
β	bulk modulus of hydraulic fluid for gap setting
δ	denotes small-perturbation signal, parameter mismatch
Ω	roller angular velocity
σ	complex plane real axis, singular value
λ	steel stress p.u. filament compression between rollers
ρ_1	steel density
ρ_2	steel resistivity
θ	angle subtended by any point in the solidification shell at roller center
θ_k	angle subtended by the kiss point at roller center
θ_l	angle subtended by the melt steel surface at roller center
Θ_r	temperature of heat sink within the rollers
Θ_s	temperature of molten steel
a^{-1}	distance separating the inside surface of the shell from internal heat sink $= \dfrac{1}{r_0 - R}$
$a_{ij}(s)$	(i,j) element of the process TFM $G(s)$
ACSE	automatic control and systems engineering
B	shell growth rate $= \dfrac{\Theta_s - \Theta_r}{\rho_1 \rho_2 H_L (r_0 - R)}$
b	speed-dependent solidification rate $= \dfrac{\Theta_s - \Theta_r}{\rho_1 \rho_2 H_L (r_0 - R)\Omega_{act}}$
$cond(M)$	condition number of matrix m
F	roller separation force
$D(s)$	polynomial common denominator of the a_{ij}
$G(s)$	process TFM
$H_1(s)$	gap setting hydraulic circuit transfer function from valve displacement to gap
$H_2(s)$	gap setting hydraulic circuit transfer function from valve displacement to roller separation force
H_L	latent heat of molten steel
$k_{dy\Omega}$	steady-state gain from roller velocity to level height
k_{dyg}	steady-state gain from gap to level height
k_{dyqi}	steady-state gain from melt input flow to level height
$k_{F\Omega}$	steady-state gain from roller velocity to roller separation force
k_{Fg}	steady-state gain from gap to roller separation force
k_{Fk}	steady-state gain from kiss height to roller separation force
$k_{k\Omega}$	steady-state gain from roller velocity to kiss height
k_{ky}	steady-state gain from level height to kiss height
m_c	gap-setting hydraulic cylinder mass
me	meniscus width ($x_g + 2x_k$)
m_r	roller mass
NP	nominal performance
NS	nominal stability
P_o	supply pressure for gap-setting hydraulic circuit
P_s, P_r	pressure at the gap-setting hydraulic cylinder
$Q(s)$	open-loop TFM (section 4), interconnection matrix (sections 5 and 6)
q_c	flow at the gap-setting hydraulic cylinder
q_d	flow at the gap-setting valve exit
q_i	melt input flow
r	distance from a given point in the solidification shell to the roller center
R	roller radius
Red%	percentage of reduction of thickness
r_k	distance from kiss point in the solidification shell to the roller center
R_l	gap-setting hydraulic valve leakage conductance
R_v^{-1}	gap-setting hydraulic valve conductance
SP	smith predictor
T	time delay
TFM	transfer function matrix
V_s, V_r	compression and expansion volumes of hydraulic fluid for gap setting
x_b	movement of gap setting hydraulic circuit support
x_c	movement of gap setting hydraulic circuit cylinder
x_g	gap between rollers
x_k	steel thickness at the kiss height
Y_k	kiss point height
Y_l	melt level height

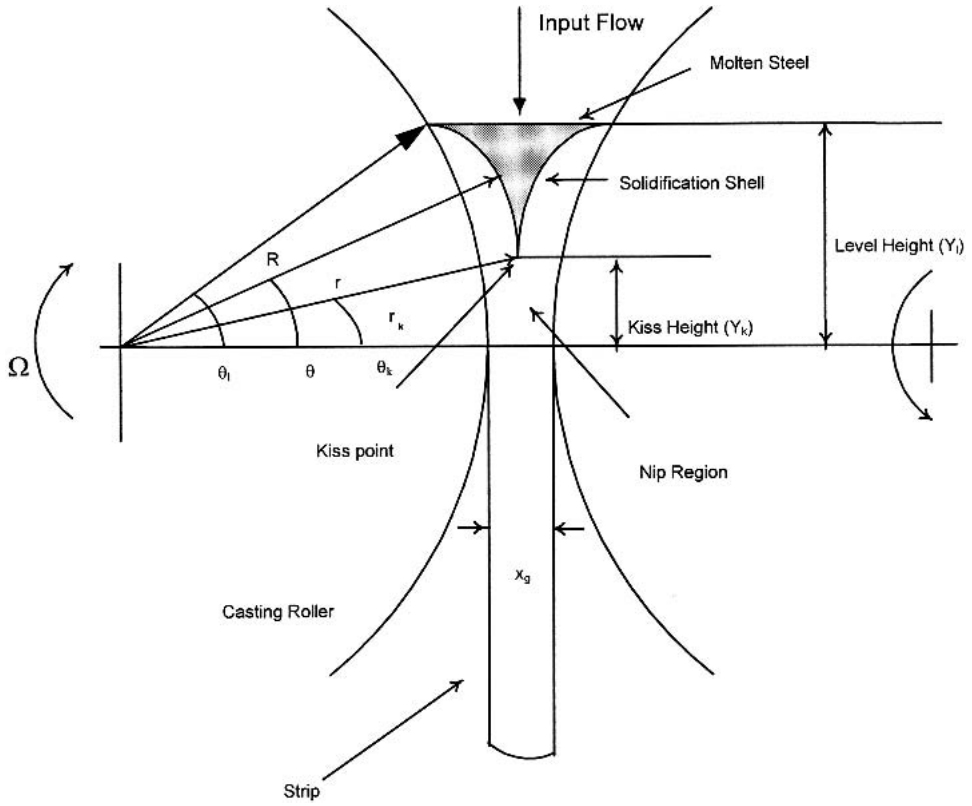

Fig. 1 Top-feeding, twin-roller, strip-casting process

which the lines touch each other is called the *kiss point*. The solid material is compressed by the rollers in the *nip region*, as shown in Fig. 1. Thus, a reaction force, called the *roller separation force*, is generated. The solid strip is produced at the exit of the rollers.

The kiss point height might be changed by varying (a) the roller gap, (b) the melt pool level, or (c) the roller speed. As the roller speed or the roller gap increases, or the pool level decreases, the kiss point is lowered. As the kiss point travels down, the problem of breakout might occur. This occurs when the kiss point does not actually exist because solidification has not been completed before molten steel leaves the rollers. In the present work, it is assumed that the kiss point is above the equator of the rollers.

3. Model of the Process

3.1 Shell Growth

In this section, the steady-state solution of the kiss height is derived via the solidification process to obtain the local gains between the different process variables.

The solidification process was simplified by assuming that the molten steel has a uniform temperature and solidifies abruptly upon the loss of latent heat, and by performing a mass balance on the solid within an infinitesimal cell at a general angle. Under these assumptions and simplifications, for an abrupt solidification interface, it is considered that the shell thickness $(R - r)$ is described by the partial differential equation:

$$\frac{\partial r}{\partial t} = \Omega\left\{\frac{\partial r}{\partial \theta} + \frac{b}{1 + a(r - R)}\right\} \qquad \text{(Eq 1)}$$

where r is the distance from the shell to the center of the roller, and $\theta_k = \theta = \theta_l$ are as in Fig. 1. The speed-dependent solidification rate is given by:

$$b = \frac{\Theta_s - \Theta_r}{\rho_1 \rho_2 H_L (r_0 - R)\Omega_{act}}$$

and Θ_s is the temperature of molten steel, Θ_r is the temperature of heat sink within the rollers, ρ_1 is the steel density, ρ_2 is the steel resistivity, H_L is the latent heat of molten steel, Ω_{act} is the actual angular velocity, and

$$a = \frac{1}{r_0 - R}$$

where a^{-1} is the distance separating the inside surface of the shell from the internal heat sink.

This equation is fundamental to a wide range of moving-bed processes (e.g., sintering, chain-grate stokers, rotary kilns, tubular reactors, and mechanized coal cutting) (Ref 21, 22), and, as mentioned, it is one of the main contributions from earlier studies on twin-roller strip casting (Ref 14, 20). Equation 1 emerges from considering the mass balance of a solid infinitesimal spatial cell in which the rate of accumulation of the solid is equated to the difference of inflow and outflow around the rollers plus the rate of deposition from the extraction of latent heat (the latter is later assumed constant, but Eq 1 allows the rate of cooling to be modulated by shell thickness via parameter a) (Ref 23).*

* The thermodynamics in this model are therefore confined to conduction and latent heat only; similar simplifications are often adopted, e.g., in distillation models.

The shell boundary conditions are defined at the molten surface to be $r = R$, and $\theta = \theta_l$. At the kiss point, shell boundary conditions are defined as $r = r_k$ and $\theta = \theta_k$. It is possible to rewrite b in the form:

$$b = \frac{B}{\Omega_{act}} \quad \text{(Eq 2)}$$

where B is a constant given by:

$$B = \frac{\Theta_s - \Theta_r}{\rho_1 \rho_2 H_L (r_0 - R)}$$

In principle, Eq 2 can be used to calculate B, but $(r_0 - R)$ is a conceptual thickness. It is more practical, however, to estimate the parameter b via calibration of theoretical and practical results.

3.2 Approximated Steady-State Formula for the Kiss Point

The exact analytic solution of the partial differential equation (Eq 1) for the shell solidification is not possible because it involves the trigonometric function $\cos\theta_k$. For small values of θ_k, it is possible to use the Taylor approximation:

$$\cos\theta_k \approx 1 - \frac{\theta_k^2}{2}$$

This allows the analytic steady-state solution for the kiss height (Y_k) to be derived under conditions of constant θ_l, Ω, b, and x_g. For the sake of simplicity, it is assumed that the thickness of the roller surface has little effect on heat conduction to the heat sinks within the rollers (i.e., $a\,[r - R] \ll 1$). Thus, under steady-state conditions ($\partial r/\partial t = 0$) Y_k solution is:

$$Y_k = -b + \sqrt{b^2 + 2\left(R + \frac{x_g}{2}\right)\left(b\theta_l - \frac{x_g}{2}\right)} \quad \text{(Eq 3)}$$

The full derivation of this is presented in Appendix A. It is possible to linearize Eq 3 by the small perturbation model technique around an operating point in the following manner:

$$\delta Y_k \cong \delta\Omega \left.\frac{\partial Y_k}{\partial \Omega}\right|_{\bar{\Omega},\bar{x}_g,\bar{Y}_l} + \delta x_g \left.\frac{\partial Y_k}{\partial x_g}\right|_{\bar{\Omega},\bar{x}_g,\bar{Y}_l} + \delta Y_l \left.\frac{\partial Y_k}{\partial Y_l}\right|_{\bar{\Omega},\bar{x}_g,\bar{Y}_l} \quad \text{(Eq 4)}$$

where δ denotes small deviation.

The following symbols will be used to represent the constants produced by the substitution of the operating conditions on the partial derivatives:

$$k_{k\Omega} = \left.\frac{\partial Y_k}{\partial \Omega}\right|_{\bar{\Omega},\bar{x}_g,\bar{Y}_l}, \; k_{kg} = \left.\frac{\partial Y_k}{\partial x_g}\right|_{\bar{\Omega},\bar{x}_g,\bar{Y}_l} \text{ and } k_{kY} = \left.\frac{\partial Y_k}{\partial Y_l}\right|_{\bar{\Omega},\bar{x}_g,\bar{Y}_l}$$

where $k_{k\Omega}$, k_{kg}, and k_{ky} are the static gains from kiss height to angular velocity, roller gap, and level height, respectively. Thus, Eq 4 can be rewritten as:

$$\delta Y_k = \delta\Omega k_{k\Omega} + \delta x_g k_{kg} + \delta Y_l k_{kY} \quad \text{(Eq 5)}$$

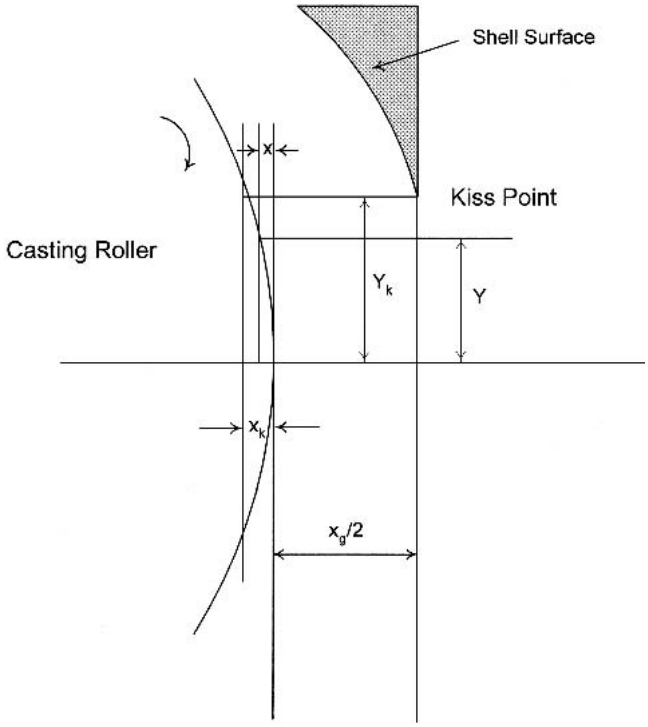

Fig. 2 Strip-casting process showing the parameters used in (Eq 6)

3.3 Steady-State Formula for Roller Separation Force

The roller separation force is a result of the compression of the solidified steel by the rollers within the nip region (Fig. 2). The solidified steel is compressed from its width (in the cross-section direction) at the kiss point to that at the roller exit (i.e., to x_g). As a simplification of what in reality is a very complex mechanical, thermodynamic, and metallurgic process, the roll separation force (F) is considered to be proportional to the integrated compressive strain within the nip-point region. Uniform distribution of steel along the rollers is also assumed. Thus:

$$F = L\lambda \int_0^{\theta_k} \frac{2(x_k - x)}{(x_g + 2x_k)} R\cos\theta d\theta \quad \text{(Eq 6)}$$

where $2(x_k - x)$ is the loss of thickness of solid steel at a particular point within the nip region, when $\theta = 0$ and $x = x_k$, and when $\theta = \theta_k$ and $x = 0$; then $(x_g + 2x_k)$ is the width at the kiss point (Fig. 2), λ is the stress per unit filament between rollers for steel, and R and L are the roller radius and length, respectively. L is assumed to be equal to 1 m. Therefore, the strip width is unity and is eliminated from force.

Using the approximations:

$x_g \ll x_k$,

$\theta_k \ll 1.0 \rightarrow \cos\theta \approx 1$, and

$$x_k \cong \frac{Y_k^2}{2R} \quad \text{(Eq 7)}$$

(proof of Eq 7 can be found in Appendix B) the following expression is obtained:

$$F = \frac{2\lambda Y_k^3}{3x_g R} \quad \text{(Eq 8)}$$

(see Appendix C for proof of Eq 8). Equation 8 can also be linearized around an operating point by the small perturbation technique:

$$\delta F = \delta Y_k \left.\frac{\partial F}{\partial Y_k}\right|_{\bar{x}_g, \bar{Y}_k} + \delta x_g \left.\frac{\partial F}{\partial x_g}\right|_{\bar{x}_g, \bar{Y}_k} \quad \text{(Eq 9)}$$

Using the following symbols it can be expressed as:

$$k_{Fk} = \left.\frac{\partial F}{\partial Y_k}\right|_{\bar{x}_g, \bar{Y}_l} \text{ and } k_{Fg} = \left.\frac{\partial F}{\partial x_g}\right|_{\bar{x}_g, \bar{Y}_l} \quad \text{(Eq 10)}$$

where k_{Fk} and k_{Fg} are the static gains from roller separation force to kiss height and roller gap, respectively.

Hence, Eq 9 can be rewritten as:

$$\delta F_k = \delta Y_k k_{Fk} + \delta x_g k_{Fg}$$

Equation 10 gives the relations $\delta F/\delta x_g$ and $\delta F/\delta Y_k$. These are not considered to be dynamic relations, and only the steady-state relations are used.

3.4 Force-Velocity Model

3.4.1 Steady-State Relation. The steady-state relation from the roller angular velocity (Ω) to the kiss point height (Y_k) is given by $k_{k\Omega}$ for small perturbations, which is obtained by partially differentiating the nonlinear approximate steady-state solution of Y_k (Eq 3) with respect to Ω (Eq 4, 5).

The small-perturbation steady-state relation from Y_k to F is given by k_{Fk}, which is obtained by partially differentiating Eq 8 with respect to Y_k (Eq 9, 10). Therefore, the small-perturbation steady-state relation from Ω to F is $k_{k\Omega}k_{Fk}$.

3.4.2 Dynamics. When a small perturbation step is applied on Ω, all of the points on the shell change their direction of travel. The kiss point will move vertically until the last point on the shell arrives at the new kiss point. Hence, the response of Y_k to a step on Ω can be considered to be a ramp of duration

$$T = \frac{\theta_l - \theta_k}{\Omega} \quad \text{(Eq 11)}$$

where $\theta_k = \tan^{-1}\left(\frac{Y_k}{R + \frac{x_g}{2}}\right)$

see Fig. 3, note that the delay time (T) is speed-dependent.

The dynamics between F and Ω can be described by (as has been done for related processes; Ref 15, 16, 20, 21):

$$G_{F\Omega}(s) = k_{F\Omega}\frac{1 - e^{-sT}}{Ts}$$

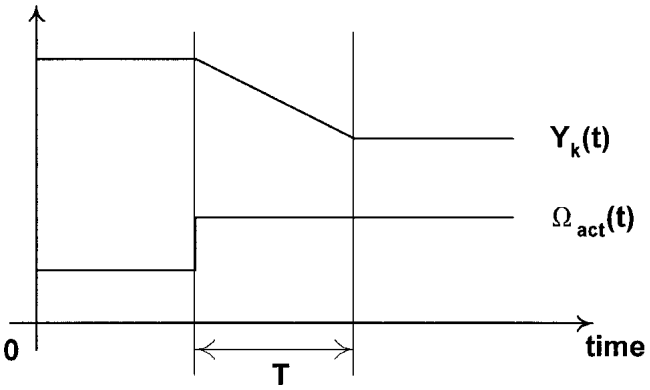

Fig. 3 Kiss height response to a step on Ω_{act}

where $k_{F\Omega}$ is as given above. Note these dynamics are defined only for the steady state under small signals.

3.5 Roller Geometry

From the roller geometry, it is possible to obtain both the steady-state relation and the dynamics from q_i, x_g, and Ω to Y_l (Fig. 4). For simplicity, the relation for the time derivative of Y_l is obtained and is given by:

$$\dot{Y}_l = \frac{q_i - q_o}{L(x_g + 2R - 2\sqrt{R^2 - Y_l^2})}$$

where q_o is the output flow.

Substituting q_o, the following expression is obtained:

$$\dot{Y}_l = \frac{q_i - \Omega R x_g L}{L(x_g + 2R - 2\sqrt{R^2 - Y_l^2})}$$

Again, this expression can be linearized in steady state around an operating point as follows:

$$\delta\dot{Y}_l = \delta q_i k_{dYq} + \delta\Omega k_{dY\Omega} + \delta x_g k_{dYg} + \delta Y_l k_{dYY}$$

where $k_{dy\Omega}$ and k_{dyq} are the static gains from the angular velocity and molten steel input flow to the first derivative of the level height, respectively.

In the following, the steady-state gain

$$k_{dYY} = \left.\frac{\partial Y_l}{\partial \dot{Y}_l}\right|_{\text{Steady State}}$$

will be assumed to be zero. The dynamics between Y_l and its time derivative is considered to be only an integrator. Thus, the dynamics are as follows:

$$Y_l(s) = [k_{dYq_i} q_i(s) + k_{dY\Omega}\Omega(s)]\frac{1}{s}$$

3.6 Level-Force Dynamics

A step on Y_l under small-perturbation conditions would cause a delayed step on Y_k with constant Ω and x_g. Thus, the dynamics are given by:

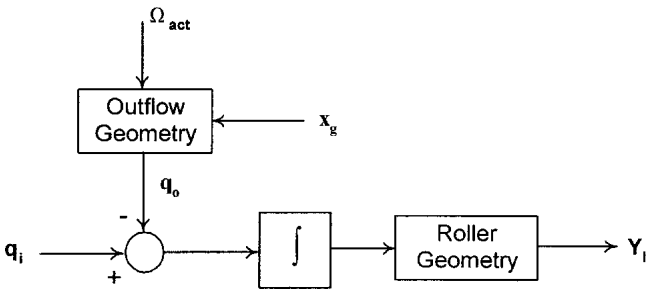

Fig. 4 Block diagram of the roller geometry

$$G_{FY}(s) = k_{FY}e^{-sT}$$

where $k_{FY} = k_{kY}k_{Fk}$, and k_{Fk} is as in Eq 9 and 10, k_{ky} is as given in Eq 4, and T is given by Eq 10.

3.7 Gap Dynamics

The gap dynamics are mainly governed by the hydraulic system, which positions the caster rollers. After linearization around an operating point of the dynamics of the hydraulic system, the block diagram (Fig. 5) is obtained. In Fig. 5, the following symbols are used: x_b is the movement of the support; x_c is the movement of the cylinder; P_0 is the supply pressure; d is the valve spool displacement; q_d is the flow at the valve exit; q_c is the flow at the cylinder; q_l is the valve leakage flow; P_s and P_r are the pressures in the cylinder; and V_s and V_r are the compression and expansion volumes of hydraulic fluid, respectively, and they account for the compressibility of the fluid.

The transfer function of the diagram in Fig. 5 is given by:

$$x_g(s) = H_1(s)d(s) + H_2(s)F(s) \quad \text{(Eq 12)}$$

where $H_1(s) = x_g(s)/d(s)$ and $H_2(s) = x_g(s)/F(s)$.

(See Appendix D for the partial derivatives for linearization of the nonlinear static relations used in this section.)

4. Multivariable Model

From the foregoing analysis, the 3 × 3 small-perturbation multivariable model of Fig. 6 is obtained with the inputs being spool valve displacement (δd), roller velocity ($\delta\Omega$), and input flow (δq_i). The outputs include the roller gap (δx_g), the roller separation force (δF), and the pool level (δY_l). (See Appendix E for a full expression of the 3 × 3 model.)

As mentioned earlier, the 3 × 3 model (Ref 14) was then simplified (Ref 15) by assuming the gap to be constant, implying that the diagonal gap controller is very tight, and that its speed of response greatly exceeds that of the dynamics driven by input melt flow, roller velocity, and the shell-forming process. This simplification was supported by time-domain simulations and experiments carried out in a real-time simulator (Ref 16), although the results of the experiments performed for large signals were consistent with some of the dynamics previously shown.

Thus, the plant is reduced to the 2 × 2 block diagram shown in Fig. 7 and has two outputs: (a) roller separation force (F); and (b) molten steel level (Y_l). It also has two inputs: (a) roller angular velocity (Ω); and (b) molten steel input flow (q_i).

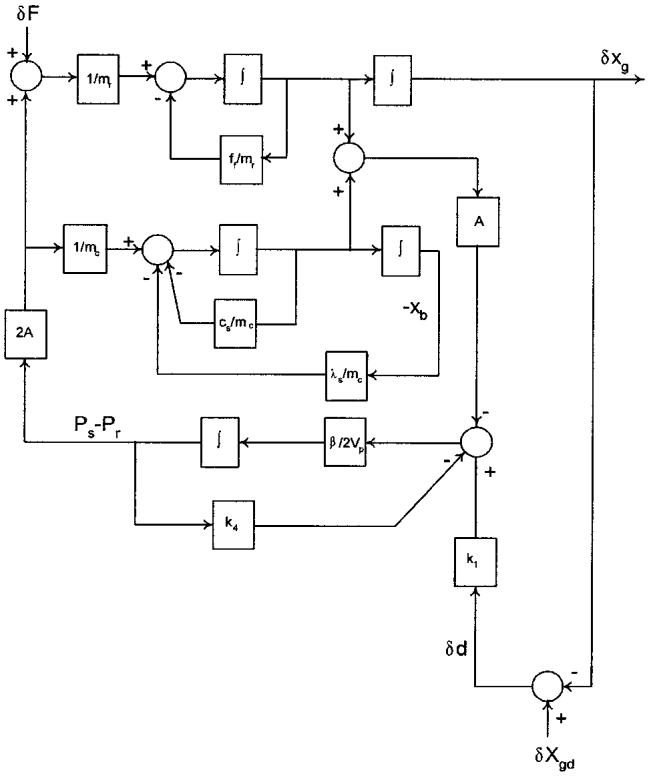

Fig. 5 Simulation diagram of the linearized hydraulic system

Therefore, the resulting transfer function matrix (TFM) of the plant $\mathbf{G}(s)$ and that used in the rest of the investigation is given by:

$$\begin{bmatrix} \delta F(s) \\ \delta Y_l(s) \end{bmatrix} = \mathbf{G}(s) \begin{bmatrix} \delta\Omega(s) \\ \delta q_i(s) \end{bmatrix} \quad \text{(Eq 13)}$$

where

$$\mathbf{G}(s) = \begin{bmatrix} k_{k\Omega}k_{Fk}\dfrac{1-e^{-sT}}{Ts} + k_{dy\Omega}k_{ky}k_{Fk}\dfrac{e^{-sT}}{s} & k_{dyq}k_{ky}k_{Fk}\dfrac{e^{-sT}}{s} \\ \dfrac{k_{dy\Omega}}{s} & \dfrac{k_{dyq}}{s} \end{bmatrix}$$

Note that the TFM $\mathbf{G}(s)$ has been derived for the special case of the feedback parameter $k_{dYY} = 0$.

Note also that the stopper valve dynamics for feeding the molten steel are not considered. The reason for this is that they are basically unknown. Therefore, for control design it is important to study the control inputs, because the actuator demands might be unachievable. However, some work on stopper valves has been reported that may be considered for future work (Ref 7).

4.1 Impact of the Controlled Variables on Strip Quality

The quality specifications are usually given in terms of thickness (which has to be within some tolerance), mechanical properties (which depends on the solidification process), and surface smoothness. It is possible to identify the factors that influence the strip quality. Strip thickness is influenced by: (a) fluctuations in the input flow rate (Ref 24); (b) contact time

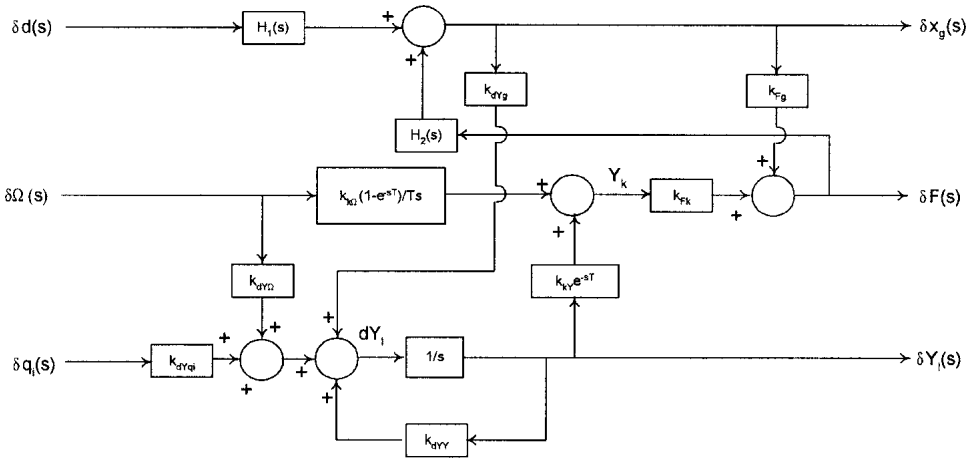

Fig. 6 Block diagram of the full linear plant

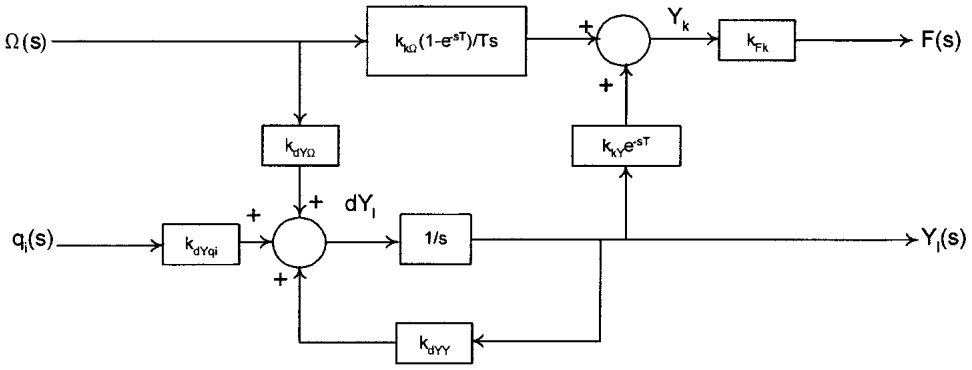

Fig. 7 Block diagram of the simplified plant

(Ref 25, 26), which depends on roller velocity, pool level, and meniscus (Ref 27); and (c) melt superheat (Ref 28).

The solidification process, and therefore the microstructure and the mechanical properties, are dependent on (a) contact time (Ref 27), (b) melt superheat (Ref 28), (c) pool level (Ref 29) (work on heat transfer modeling assuming that a constant pool level has been performed) (Ref 13); (d) input flow (Ref 26); (e) strip thickness (Ref 27); and (f) heat transfer coefficient, which can be changed by: casting velocity (Ref 13, 27, 30) and roller separation force (Ref 29).

The strip surface depends on: (a) casting speed (Ref 27); (b) uneven distribution of mass flow (Ref 31); (c) solidification process (Ref 28, 32); (d) nonparallel axes of the rollers (Ref 28); and (e) fluctuations in the gap between rollers (Ref 29).

From the survey above, and considering the three controlled variables of the proposed model (F, Y_l, and x_g), it can be concluded that a controller based on a model of this type can give control on the strip quality. As mentioned above, the strip thickness loop was neglected for the simplified 2 × 2 model.

5. Multivariable Characteristics

5.1 Calibration of the Shell-Growing Process

Before proceeding with the analysis, the shell-growing process model (i.e., B) was calibrated using data from a pure static model that was used in the industrial site. This model has been used in the plant to estimate some variables for engineering purposes, and it has been experimentally validated. Therefore, it is considered that the static model represents the steady-state behavior of the process quite well.

Table 1 shows the calibration data, Y_k, the meniscus ($m_e = x_g + 2x_k$ [x_k = thickness at Y_k]), and the thickness reduction percentage (Red%). The intermediate value of casting speed (25 m/min, $\Omega = 0.18$ rad/s) was chosen, having $B = 0.00247$ m/rad. However, due to the low-level conditions, higher casting speeds were not feasible, keeping x_g and F nominal, and assuming that there are x_g and F controllers that will keep them constant when the level is decreased, so roller speeds will be decreased. Because of roller curvature, low-level conditions are more critical than high-level conditions, smaller changes in input flow cause larger changes in pool level, and therefore in force.

5.2 Multivariable Poles and Zeros

Note the defined methods to obtain the multivariable poles and zeros are suitable for rational systems. However, the application will proceed, bearing in mind this important limitation. The development of special methods to obtain the multivariable poles and zeros of a time-delay system is out of the scope of the present application-focused investigation. The rational system definition is used here on the assumption that the strip caster might be approximated by such a system, at least over a range of frequencies.

The Smith-McMillan form of the strip caster, denoted by

Table 1 Parameter *B* calibration data

Peripheral speed, m/min (mm/s)	Parameter *B*	Sheffield model predictions			Static model predictions		
		Y_k, mm	Red%	m_e, mm	Y_k, mm	Red%	m_e, mm
30 (500)	2.06	5.77	2.089	4.26	5.77	2.089	4.26
25 (416.7)	2.47	9.78	2.255	11.31	11.64	2.361	15.29
20 (333.33)	3.09	14.8	2.58	22.48	16.16	2.697	25.84

G_{SM}, was obtained by the method revised by Maciejowski (Ref 33). It is given by:

$$G_{SM}(s) = \frac{1}{s}\begin{bmatrix} k_{dY\Omega} & 0 \\ 0 & -\dfrac{k_{dYq}k_{k\Omega}k_{Fk}(1-e^{-sT})}{k_{dY\Omega}T} \end{bmatrix}$$

As expected, the method based on the minors of the TFM (Ref 34) yields the same results. The determinant of the plant $G(s)$ is given by:

$$\left|G(s)\right| = k_{k\Omega}k_{Fk}k_{dyq}\frac{(1-e^{-sT})}{Ts^2}$$

From $G_{SM}(s)$ or $|G(s)|$, it is possible to see that the poles of $G(s)$ are those values of s for which the function $(1 - e^{-sT})$ approaches infinity as well as the two poles introduced by the integrators. The zeros of $G(s)$ are those values of s that make $(1 - e^{-sT})$ equal to zero.

When $\sigma = -\infty$, the function $(1 - e^{-sT})$ is equal to $1 - \infty \angle -j\omega T$. Consequently, $G(s)$ has an infinite number of poles at $-\infty$ plus the two poles at the origin introduced by the integrators. When $\sigma = 0$ and $\omega = n2\pi/T$, where n is an integer, the function $(1 - e^{-sT})$ is equal to zero, and therefore $G(s)$ has an infinite number of zeros on the $j\omega$-axis for every $\omega = 2\pi/T$, including the origin. Both findings are in accordance with the initial expectations due to presence of the delays.

The presence of the zeros on the $j\omega$-axis (assuming that the methods are valid for the model of the strip caster presented here) may cause a limitation on performance, because for certain directions of the input at the frequencies where the zeros are located, the gain is zero. Limitations on performance are also expected due to the presence of the time delays (Ref 34).

5.3 Interaction Levels

As mentioned earlier, the TFM (Eq 13) was found to be highly interactive (i.e., high diagonal dominance ratios) (Ref 33). Row 1 diagonal dominance ratios for two different pool levels of the scaled plant are depicted in Fig. 8. Row 2 diagonal dominance ratios are not shown because they are equal to 1 for all frequencies. Figure 9 shows the column diagonal dominance ratios for two different pool levels.

It can be observed that the largest and most critical of all these ratios is that of column 2, which corresponds to element g_{12}, the relationship between roll separation force and pool level. Although constant, it is considerably larger than unity (i.e., more than 100%) and increases as the pool level decreases. This means that at low pool levels the interaction between pool level and force is more critical. The dominance ratio for row 2 is equal to unity (100%) and is also undesirable. The ratios for row 1 and column 2 seem to be low; however,

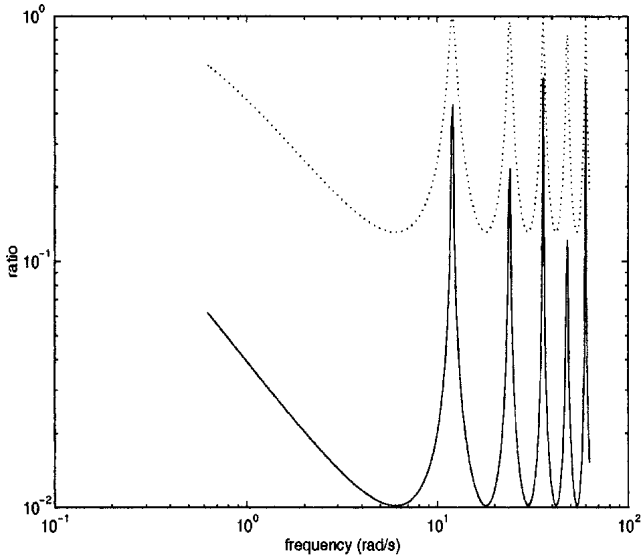

Fig. 8 Comparisons among row 1 diagonal dominance ratio, nominal plant (solid line) and low-fill (25%) operating conditions (dotted line)

they have high-frequency components, which might be difficult to cope with for a diagonal proportional plus integral plus derivative (PID) controller. On the other hand, the high-frequency peaks might be cut off by the simulation software resolution, being larger than they look in the plot. However, the row 2 ratio becomes significant for low pool levels, and, aside from the aforementioned peaks, which reach unity, the lowest values in between the peaks are 0.1 (10%). Therefore, it can be concluded that the system is highly interactive and that a diagonal controller might not be enough to reject such interactions.

5.4 Singular Values

Figures 10 and 11 depict the singular values and the minimized condition number (i.e., the condition number for the scaled plant is called the *minimized condition number*) at two different pool levels. In the figures, $\overline{G}$ denotes the scaled plant. The condition number has been interpreted as robust performance sensitive. Plants with large condition numbers are said to be ill-conditioned plants because they may present difficulties in attaining robustness (Ref 34). The reason for this is that the lowest singular value $[\underline{\sigma}(\overline{G})]$ might be too small, and, therefore, the plant has a low gain for a certain input direction that is highly sensitive to input direction uncertainties. It should be noted that the minimized condition number is large for all frequencies and for both pool levels. This is because $\underline{\sigma}(\overline{G})$ is small (i.e., <1) for all frequencies. Therefore, it can be concluded that the multivariable model of the strip-casting process is ill conditioned.

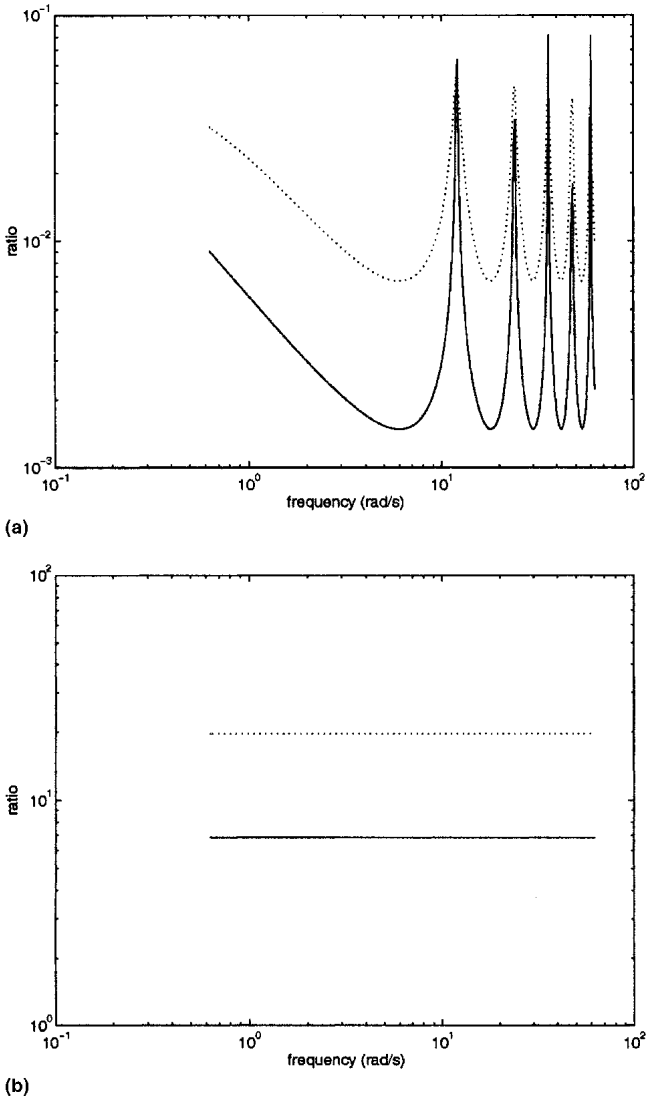

Fig. 9 Comparisons of the column diagonal dominance ratio, nominal plant (solid line), low-fill (25%) operating conditions (dotted line): (a) column 1; and (b) column 2

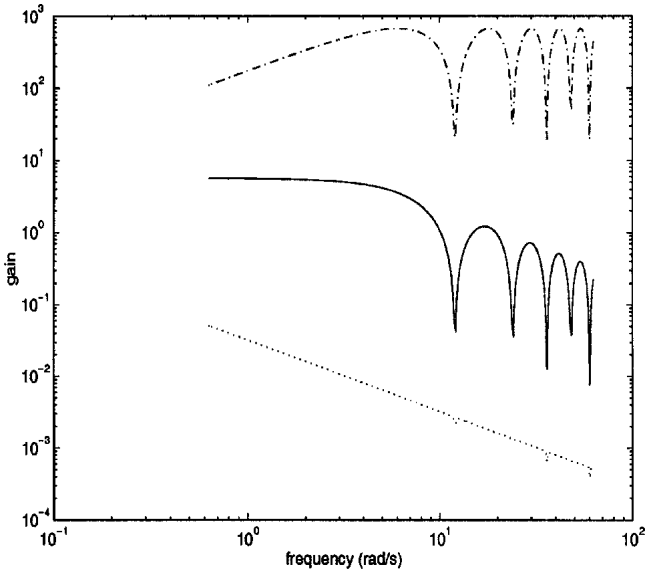

Fig. 10 $\bar{\sigma}(\overline{G})$ (solid line), $\underline{\sigma}(\overline{G})$ (dotted line), and minimized $cond(\overline{G})$ (dashed-dotted line)

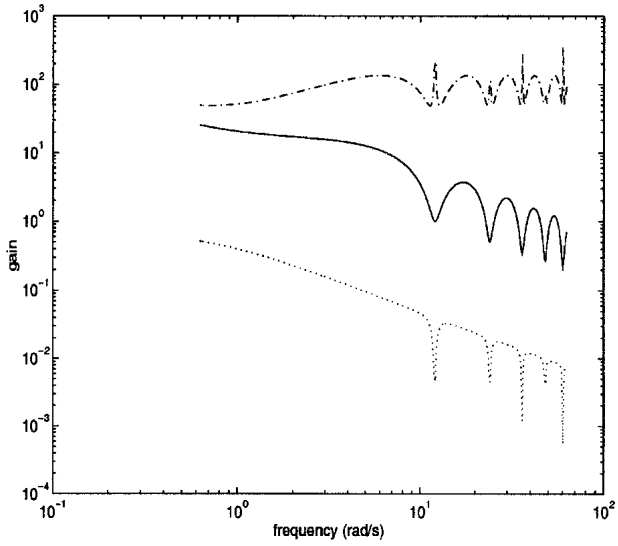

Fig. 11 $\bar{\sigma}(\overline{G})$ (solid line), $\underline{\sigma}(\overline{G})$ (dotted line), and minimized $cond(\overline{G})$ (dashed-dotted line), for the low-fill (25%) operating point

A stability analysis of the simplified 2 × 2 small-perturbation multivariable model via the characteristic loci can be found in (Ref 16). It was concluded that the process might be stabilized with a simple diagonal proportional controller; therefore, according to the previous multivariable analysis, it was concluded that the main difficulties with this plant are the limitation on performance imposed by zeros on the $j\omega$-axis, the interaction levels, and the possible sensitivity to uncertainties, as shown by the high minimized condition number. The simplified 2 × 2 small-perturbation multivariable model has been successfully used for the design of several diagonal and multivariable control systems (Ref 15, 16).

6. Conclusions and Future Work

After linearization around an operating point, a 3 × 3 small-perturbation multivariable model of the twin-roller strip caster that is suitable for control design was obtained. This model captures the dynamic characteristics of the process (i.e., interactions, time delays, and nonlinearities) when studying different operating points. The controlled variables proposed in the model influence the factors that govern the strip quality.

The 3 × 3 TFM was simplified into a 2 × 2. The multivariable poles and zeros of the 2 × 2 TFM have been obtained via the Smith-McMillan method, assuming that a rational approximation of the strip caster is possible. The presence of time delays and zeros on the $j\omega$-axis may cause limitations on performance.

The plant was found to be highly interactive via the diagonal ratios of the multivariable models. On the other hand, due to the high minimized condition number and the low singular value of $\underline{\sigma}(\overline{G})$ for two different pool levels, the plant can be considered to be ill conditioned, and, hence, it is expected to present problems for attaining robustness.

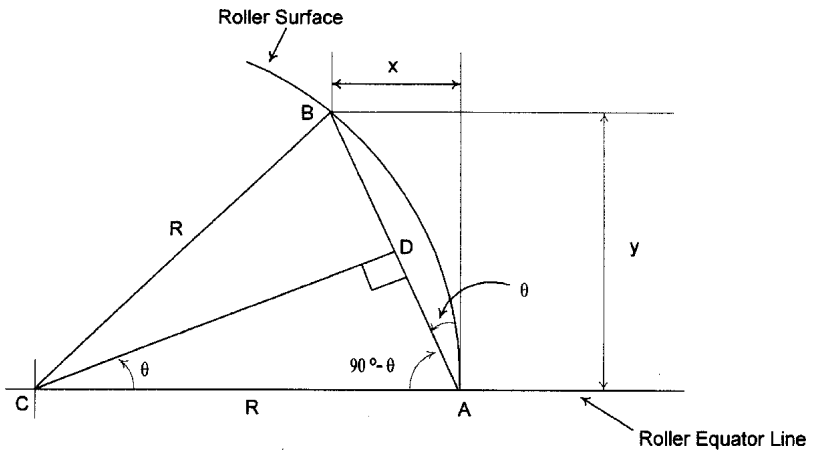

Fig. B1 Trigonometry for the derivation of the relationship between solid thickness and height within the nip region

Appendix A. Approximate Analytic Solution for Steady-State Kiss Height

In the steady state, the shell thickness partial differential (Eq 1) can be written as:

$$\frac{\partial r}{\partial \theta} = -b$$

$$r = -b\theta + \mathrm{c}$$

where c is a constant.

Applying the boundary condition at the molten surface, $r = R$, at $\theta = \theta_l$, gives the constant c as:

$$\mathrm{c} = R + b\theta_l$$

Substituting conditions at the kiss point:

$$r_k = \frac{d}{\cos \theta_k}$$

where $d = R + \frac{x_g}{2}$

and using Taylor approximation for $\cos \theta_k$, gives

$$\frac{d}{1 - \frac{\theta_k^2}{2}} = -b\theta_k + \mathrm{c}$$

and because $\theta_k \ll 1.0$, then

$$d\left(1 - \frac{\theta_k^2}{2}\right) \approx -b\theta + \mathrm{c}$$

Rearranging gives a quadratic polynomial in θ_k,

$$\frac{d}{2}\theta_k^2 + b\theta_k + (d - \mathrm{c}) = 0$$

Solving gives:

$$\theta_k = \frac{-b \pm \sqrt{b^2 - 2d(d - \mathrm{c})}}{d}$$

Then, the kiss height, Y_k, is given by:

$$Y_k \approx d\theta_k = -b + \sqrt{b^2 - 2d(d - \mathrm{c})}$$

Substituting for d, and c gives

$$Y_k \cong -b + \sqrt{b^2 + 2\left(R + \frac{x_g}{2}\right)\left(b\theta_l - \frac{x_g}{2}\right)}$$

Thus, proving Eq 3.

Appendix B. Approximate Relation Between Solid Thickness and Height in the Nip Region

Consider the portion of the nip region, as illustrated in Fig. 1 and Fig. B1.

The relationship between x (and hence between the width $x_k = 2x + x_g$) and the height y (and Y_k) can be derived by straightforward trigonometry:

$$\tan \theta = x/y$$

where y is the height from the roller equator to a given point within the nip region, and x is as given in Fig. B1.

Also, $\tan \theta = DA/CD$ or $\sin \theta = DA/R$

$$2DA = \sqrt{x^2 + y^2}$$

$$\sin \theta = \frac{\sqrt{x^2 + y^2}}{2R}$$

$$\cos \theta = \frac{\sqrt{4R^2 - (x^2 + y^2)}}{2R}$$

$$\tan\theta = \sqrt{\frac{x^2+y^2}{4R^2-(x^2+y^2)}}$$

$$\frac{x^2}{y^2} = \frac{x^2+y^2}{4R^2-(x^2+y^2)}$$

Now let $X = x^2$, $Y = y^2$ and $4R^2 = Z$

$$\frac{X}{Y} = \frac{X+Y}{Z-(X+Y)}$$

$$X^2 + X(2Y-Z) + Y^2 = 0$$

$$X = \frac{-(2Y-Z) \pm \sqrt{Z^2-4YZ}}{2}$$

substituting the original variables and after simplification it is obtained:

$$x^2 = 2R^2 - y^2 \pm 2R\sqrt{R^2-y^2}$$

If $y = 0$, then $x^2 = 2R^2 \pm 2R^2$, $x = 0$ or $2R$, which is not possible; therefore, the negative sign is the practical solution:

$$\left(\frac{x}{R}\right)^2 = 2 - \left(\frac{y}{R}\right)^2 - 2\sqrt{1-\left(\frac{y}{R}\right)^2}$$

Considering the following equation:

$$w = 2 - u - 2\sqrt{1-u}$$

where $w = (x/R)^2$ and $u = (y/R)^2$

$$\text{let } f(u) = 2\sqrt{1-u}$$

$$\text{now } \frac{df}{du} = -\frac{1}{\sqrt{1-u}} \qquad \frac{d^2f}{du^2} = \frac{1}{2(1-u)^{1.5}}$$

then:

$$\left.\frac{df}{du}\right|_{u=0} = -1 \qquad \left.\frac{d^2f}{du^2}\right|_{u=0} = -\frac{1}{2}$$

using Taylor's theorem,

$$f(u) \cong f(0) + \left.\frac{df}{du}\right|_{u=0} u + \frac{1}{2}\left.\frac{d^2f}{du^2}\right|_{u=0} u^2$$

it can be expressed as:

$$f(u) \cong 2 - u - \frac{u^2}{4}$$

Thus

$$w \cong \frac{u^2}{4}$$

and hence:

$$\left(\frac{x}{R}\right)^2 \cong \frac{1}{4}\left(\frac{y}{R}\right)^2 \text{ and } x \cong \frac{y^2}{2R}$$

With this, the approximate relationship between the solid thickness and height in the nip region is demonstrated.

Appendix C. Approximate Relation Between Roll Separation Force and Kiss Height

If $x_g \ll x_k$, $\theta_k \ll 1.0$, and hence, $\cos\theta \approx 1$ (Fig. 2 and B1), Eq 6

$$F = L\lambda \int_0^{\theta_k} \frac{2(x_k - x)}{(x_g + 2x_k)} R\cos\theta d\theta$$

can be approximated by:

$$F \approx L\lambda \int_0^{\theta_k} \frac{2(x_k - x)}{x_g} R d\theta$$

because from the relation between the solid thickness and kiss height: $x_k \cong Y_k/R$ and $x \cong Y/R$, then:

$$F \approx \frac{L\lambda}{x_g} \int_0^{Y_k} \frac{(Y_k^2 - y^2)}{R} dy$$

now integrating between limits Eq 8 is obtained.

Appendix D. Partial Derivative for the Small-Perturbation Model

$$k_{k\Omega} = \frac{\partial Y_k}{\partial \Omega} = \frac{B}{\Omega^2} - \frac{\sqrt{2}B\left\{\Omega[x_g+2R]\sin^{-1}\left(\frac{Y_1}{R}\right) + 2B\right\}}{2\Omega^2\sqrt{2B\Omega[x_g+2R]\sin^{-1}\left(\frac{Y_1}{R}\right) - \Omega^2 x_g^2 - 2R\Omega^2 x_g + 2B^2}}$$

$$k_{kY} = \frac{\partial Y_k}{\partial Y_1} = \frac{\sqrt{2}B[x_g+2R]}{2\sqrt{\{2B\Omega[x_g+2R]\sin^{-1} - \Omega^2 x_g^2 - 2R\Omega^2 x_g + 2B^2\}(R^2 - Y_1^2)}}$$

$$k_{Fk} = \frac{\partial F}{\partial Y_k} = \frac{2\lambda L Y_k^2}{x_g R}$$

$$k_{Fg} = \frac{\partial F}{\partial x_g} = -\frac{6\lambda L Y_k^3}{9x_g^2 R}$$

$$k_{dy\Omega} = \frac{\partial \dot{Y}_1}{\partial \Omega} = \frac{x_g R}{x_g + 2R - 2\sqrt{R^2 - Y_1^2}}$$

$$k_{\mathrm{dyq_i}} = \frac{\partial \dot{Y}_1}{\partial q_i} = \frac{1}{L[x_g + 2R - 2\sqrt{R^2 - Y_1^2}}$$

$$k_{\mathrm{dy\Omega}} = \frac{\partial \dot{Y}_1}{\partial x_g} = \frac{\Omega R(x_g + 2R - 2\sqrt{R^2 - Y_1^2}) - q_i - \Omega x_g R}{[x_g + 2R - 2\sqrt{R^2 - Y_1^2}]^2}$$

Appendix E. Transfer Function Matrix of the Full 3 × 3 Plant

If the TFM is considered to be of the form:

$$G(s) = \frac{A(s)}{B(s)}$$

where $A(s)$ is a polynomial matrix of numerators and $B(s)$ is scalar polynomial denoting a greater common denominator.

The TFM can be expressed as:

$$G(s) = \frac{1}{D(s)} \begin{bmatrix} a_{11}(s) & a_{12}(s) & a_{13}(s) \\ a_{21}(s) & a_{22}(s) & a_{23}(s) \\ a_{31}(s) & a_{32}(s) & a_{33}(s) \end{bmatrix}$$

Taking the scalar transfer functions involved in the block diagram given in Fig. 6, and after algebraic manipulation to obtain a common denominator, the elements of the TFM are given by the following expressions.

$$D(s) = s[s(1 - k_{\mathrm{Fg}}H_2(s)) - H_2(s)K_1e^{-s\mathrm{T}}][s - H_2(s)(sk_{\mathrm{Fg}} + K_1e^{-s\mathrm{T}})]$$

$$a_{11}(s) = s[s(1 - k_{\mathrm{Fg}}H_2(s)) - H_2(s)K_1e^{-s\mathrm{T}}]sH_2(s)$$

$$\begin{aligned} a_{12}(s) &= s[s - H_2(s)(sk_{\mathrm{Fg}} + K_1e^{-s\mathrm{T}})][k_{k\Omega} + e^{-s\mathrm{T}}(k_{\mathrm{dY}\Omega}k_{\mathrm{kY}} \\ &\quad - k_{k\Omega})]H_2(s)k_{\mathrm{Fk}}\, a_{13}(s) \\ &= s[s - H_2(s)(sk_{\mathrm{Fg}} + K_1e^{-s\mathrm{T}})]H_2(s)K_2e^{-s\mathrm{T}} \end{aligned}$$

$$a_{21}(s) = s[s(1 - k_{\mathrm{Fg}}H_2(s)) - H_2(s)K_1e^{-s\mathrm{T}}](sk_{\mathrm{Fg}} + K_1e^{-s\mathrm{T}})H_1(s)$$

$$a_{22}(s) = s[s - H_2(s)(sk_{\mathrm{Fg}} + K_1e^{-s\mathrm{T}})][k_{k\Omega} + e^{-s\mathrm{T}}(k_{\mathrm{dY}\Omega}k_{\mathrm{kY}} - k_{k\Omega})]$$

$$a_{23}(s) = s[s - H_2(s)(sk_{\mathrm{Fg}} + K_1e^{-s\mathrm{T}})]K_2e^{-s\mathrm{T}}$$

$$a_{31}(s) = s[s(1 - k_{\mathrm{Fg}}H_2(s)) - H_2(s)K_1e^{-s\mathrm{T}}]H_1(s)k_{\mathrm{dYg}}$$

$$\begin{aligned} a_{32}(s) &= [s - H_2(s)(sk_{\mathrm{Fg}} + K_1e^{-s\mathrm{T}})][sk_{\mathrm{dY}\Omega}(1 - H_2(s)k_{\mathrm{Fg}}) \\ &\quad + H_2k_{k\Omega}k_{\mathrm{dYg}}k_{\mathrm{Fk}}(1 - e^{-s\mathrm{T}})] \end{aligned}$$

$$a_{23}(s) = s[s - H_2(s)(sk_{\mathrm{Fg}} + K_1e^{-s\mathrm{T}})][k_{\mathrm{dYq}}(1 - k_{\mathrm{Fg}}H_2(s))]$$

where the parameters are given in Appendix C, $K_1 = k_{\mathrm{dYg}}k_{\mathrm{kY}}k_{\mathrm{Fk}}$, $K_2 = k_{\mathrm{dYq}}k_{\mathrm{Fk}}k_{\mathrm{kY}}$, H_1 is the hydraulic transfer function $x_g(s)/d(s)$, and H_2 is the hydraulic transfer function $F(s)/d(s)$ (Eq 12 and Fig. 5).

References

1. J.W. Hlinka, J.A. Burgo, and T.J. Conatry, Modelling and Design of Twin-Roll Casters, *Proceedings of a International Symposium on Casting of Near Net Shape Products: Casting of Near Net Shape Product,* The Metallurgical Society, Warrendale, PA, 1988, p 115-132
2. R.K. Pitler, An Overview of Coil Casting, Production of Flat Coilable Product Directly from Molten Metal, *Proceedings of a International Symposium on Casting of Near Net Shape Products: Casting of Near Net Shape Product,* The Metallurgical Society, Warrendale, PA, 1988, p 381-391
3. K. Shibuya and M. Ozawa, Strip Casting Techniques for Steel, *ISIJ Int.,* Vol 31, 1991, p 661-668
4. A. L. Robson and G. L. Thompson, Direct Casting of Thin Strip, *Mater. World,* Vol 3, 1995, p 222-224
5. P. Tolve, M. Ghersi, and R. Capotosti, Twin-Roll Strip Casting Experimental Trials, *International Conference on New Smelting Reduction and Near Shape Casting Technologies for Steel,* Pohang, Korea, Research Institute of Industrial Science and Technology (RIST), 1990, p 653-666
6. S. Bernhard, M. Enning, and H. Rake, Automation of a Laboratory Plant for Direct Casting of Thin Steel Strips, *Control Eng. Pract.,* Vol 2, 1994, p 961-967
7. F. Simon, S. Bernhard, and H. Rake, Gain Scheduled PI-Control of Strip Casting Plant, *IFAC Conference on Control of Industrial Systems,* Belfort, France, International Federation of Automatic Control, Vol 3, 1997, p 1179-1184
8. M.G. Joo, Y.H. Kim, and T. Kang, Stable Adaptive Fuzzy Control of Molten Steel Level in the Strip Casting Process, *Institute of Electrical Engineers Proceedings Control Theory and Application,* Vol 149, 2002, p 357-364
9. D. Lee, S. J. Lee, and T. Kang, Adaptive Fuzzy Control of the Molten Steel Level in a Strip-Casting Process, *Control Eng. Pract.,* Vol 4, 1996, p 1511-1520
10. H. Keum-Shik, K. Jeom-Goo, and M. Tomizuka, Control of Strip Casting Process: Decentralization and Optimal Roll Force Control, *Control Eng. Pract.,* Vol 9, 2001, p 933-945
11. H. Keum-Shik, K. Sung-Hoon, and L. Kyo-Il, An Integrated Control of Strip Casting Process by Decentralization and Optimal Supervision, *Proceedings of the American Control Conference,* Philadelphia, PA, Institute of Electrical and Electronic Engineers (IEEE), Vol 2, 1998, p 723-727
12. F. Simon, H. Rake, R. Kopp, L. Hentschel, and W. Schmitz, Modeling of Force and Torque of Strip Casting Process, *IFAC Conference on Automation in Mining, Mineral Metal Processing,* Cologne Germany. Sponsored by the IFAC, 1998, p 87-92
13. C.A. Santos, J.A. Spim, and A. Garcia, Modeling of Solidification Process in Twin Roll Strip Casting, *J. Mater. Proc. Technol.,* Vol 102, 2000, p 33-39
14. J.B. Edwards and D.A. Linkens, "Control of Roll Separation Force in a Continuous Strip Caster by Manipulation of Casting Speed: Analysis for Control Design," Confidential Industrial Report (1991) (91/1), The University of Sheffield, ACSE, 1991
15. S.M. Hargrave, "Aspect of Multivariable Control for Continuous Casting," Master's thesis, The University of Sheffield, 1992
16. A. Cavazos-Gonzalez, "Multivariable Control of Moving Bed Processes: An Application to Steel Making," Ph.D. dissertation, The University of Sheffield, 1996
17. J.B. Edwards and D.H. Owens, 1st-Order-Type Models for Multivariable Process Control, *Proc. IEE,* Vol 124, 1977, p 1083-1088
18. J.C. Doyle, Structured Uncertainty in Control System Design, *Proceeding of 24th IEEE Conference on Decision and Control,* Fort Lauderdale, FL, IEEE, 1985, p 260-265
19. G. Alevisakis and D.E. Seborg, An extension of the Smith Predictor Method to Multivariable Linear Systems Containing Time Delays, *Int. J. Control,* Vol 3, 1973, p 541-551
20. J.B. Edwards, I.C. Willis, J.M. Goorney, R.J. Hollands, and S.M. Hargrave, "A Simulator for Continuous Strip Casting Machine," Confidential Industrial Report (1992) (92/2), The University of Sheffield, ACSE, 1992
21. J.B. Edwards and S.M. Hargrave, Multivariable Control of a Variable-Speed Distributed Industrial Process with Manipulable Boundary Conditions, *Proceedings of the AMST94, 5th International Symposium on Application of Multivariable System Techniques,* Bradford, UK, IEEE, 1994, p 173-182
22. J.B. Edwards, J.M. Goorney, R. Hollands, and H. Mistry, Compensation of Variable Speed Process Dynamics, *Canadian Conference and Exhibition on Industrial Automation,* Montreal, Canada, Instrument Society of America, Vol 1, 1992, p 10.21-10.25

23. H. Nicholson, *Modelling of Dynamical Systems,* Vol 1, Peter Peregrinus, Ltd., Stevenage, U.K., 1980
24. S. Miyake, F. Kogiku, M. Yukumoto, M. Ozawa, T. Kan, and A. Momoo, *Melt Flow Control in Twin-Roll Casting, Proceedings of a International Symposium on Casting of Near Net Shape Products, in Casting of Near Net Shape Product,* The Metallurgical Society, Warrendale, PA, 1988, p 621-628
25. K. Miyazawa, T. Mizoguchi, M. Nakamura, and T. Ohashi, The Formation of Thin Steel Strip in Laboratory-Scale Twin-Roll Casting, *Proceedings of an International Symposium on Casting of Near Net Shape Products,* The Metallurgical Society, Warrendale, PA, 1988, p 629-643
26. A. Kasama, S. Tanaka, Y. Itoh, H. Kajioka, K. Yanagi, and K. Sasaki, Twin Drum Casting Process for Stainless Steel Strip, *International Conference on New Smelting Reduction and Near Shape Casting Technologies for Steel,* Pohang, Korea. Sponsored by RIST, 1990, p 643-652
27. K. Miyazawa, T. Mizoguchi, Y. Ueshima, and S. Mizoguchi, The Fundamental Phenomena Determining Strip Quality in Twin-Roll Casting Process, *International Conference on New Smelting Reduction and Near Shape Casting Technologies for Steel,* Pohang, Korea. Sponsored by RIST, 1990, p 745-753
28. J.C. Yoon, D.G. Choo, T. Kang, and Y.K. Shin, The Solidification Characteristic of AISI 304 Stainless Steel by Twin-Roll Strip Casting Process, *International Conference on New Smelting Reduction and Near Shape Casting Technologies for Steel,* Pohang, Korea. Sponsored by RIST, 1990, p 604-616
29. S. Miyake, H. Yamane, M. Yukumoto, and M. Ozawa, Strip Quality of Highly Alloyed Metals by Twin Roll Casting, *ISIJ Int.,* Vol 31, 1991, p 689-695
30. S. Thiem, W. Löser, and M. Jurisch, Solidification Modelling of Microstructure in Twin-Roller Thin Strip Casting of Stainless Steels, *Steel Res.,* Vol 64, 1993, p 307-312
31. T. Tohge, K. Amano, T. Maruyama, and M. Noda, Experimental Study of Strip Casting Process with Twin-Roll Caster, *International Conference on New Smelting Reduction and Near Shape Casting Technologies for Steel,* Pohang, Korea. Sponsored by RIST, 1990, p 617-626
32. T. Kusakawa and T. Okamura, Special Thin Strip Casting of Ferrous Materials and Their Characteristics, *International Conference on New Smelting Reduction and Near Shape Casting Technologies for Steel,* 1990, p 560-569
33. J.M. Maciejowski, *Multivariable Feedback Design,* Addison-Wesley Publishers Ltd., Wokingham, U.K, 1989
34. S. Skogestad and I. Postlethwaite, *Multivariable Feedback Control,* John Wiley & Sons, West Sussex, U.K., 1996